

# Introducing numerical bounds to improve event-based neural network simulation

Bruno Cessac, Olivier Rochel, Thierry Viéville

LJAD <http://math1.unice.fr> & INRIA Cortex & Odyssee <http://inria.fr>

## Abstract

Although the spike-trains in neural networks are mainly constrained by the neural dynamic itself, global temporal constraints (refractoriness, time precision, propagation delays, ..) are also to be taken into account. These constraints are revisited in this paper and their consequences are developed at the simulation level.

We first introduce these constraints, review their obvious consequence in terms of the amount of information in a spike train and discuss in details the impact at the level of the network dynamics, thanks to recent theoretical results. The goal of this first part is to provide a comprehensive view of the related technical results.

Then, the consequences of these time constraints at the simulation level are developed, showing event-based simulation of time-constrained networks can be impacted and somehow improved in this context: the underlying data-structures are strongly simplified, while event-based and clock-based mechanisms can be easily mixed. These ideas are applied to punctual conductance based generalized integrate and fire neural network simulation, while spike-response model simulation is also revisited within this framework. These mechanisms are compared using existing benchmarks.

**Key Words** Spiking network. Neural code. Simulation.

## 1 Introduction

Let us consider biological models of cortical maps (Koch & Segev, 1998; Dayan & Abbott, 2001), in a context where the spiking nature of neurons activity is made explicit (Gerstner & Kistler, 2002), either from a biological point of view or for computer simulation. From the detailed Hodgkin-Huxley model (Hodgkin & Huxley, 1952), (still considered as the reference but unfortunately intractable when considering neural maps), back to the simplest integrated and fire (IF) model (see e.g. (Gerstner & Kistler, 2002)), a large family of continuous-time models have been produced, often compared with respect to their (i) biological plausibility and their (ii) simulation efficiency.

### **Biological plausibility of neural network models.**

Biological plausibility at the neuron level is understood as the capability to reproduce what is observed at the cell level, often considering in-vitro experiments (Koch & Segev, 1998). This is a questionable point of view as shown in recent experiments in V1 (Frégnac, 2003, 2004) where it appears that a single-cell observation highly differs between in-vitro and in-vivo conditions. Biological plausibility at the neural network level is understood as the capability to reproduce what is observed regarding e.g. the cortical map activity (Carandini et al., 2005). This includes predicting the response not only to specific artificial but also natural stimuli: this means, for V1, taking natural image sequences input shifted by eye movements into account (Baudot, 2007), after the retinal and

LGN processing (see e.g. (Simoncelli & Olshausen, 2001) for a discussion about information processing in these structures).

As far as this contribution is concerned, we consider a weaker notion of biological plausibility: a simulation is biologically plausible if it verifies an explicit set of constraints observed in the biology. More precisely, we are going to review and discuss a few global time constraints and develop their consequences at the simulation level. It appears here that these biological temporal limits are very precious quantitative elements, allowing us on one hand to bound and estimate the coding capability of the system and on the other hand improve simulations.

### **Simulation efficiency of neural network simulators**

Simulation efficiency is a twofold issue of precision and performances. See (Brette et al., 2007) for a recent review about both event-based and clock-based simulation methods.

Regarding precision, event-based simulations, in which firing times are not regularly discretized but calculated event by event at the machine precision level, provides (in principle) an *unbiased* solution. On the reverse, it has been shown that a regular clock-based discretization of the continuous neural system may introduce systematic errors (Cessac & Samuelides, 2007), with drastic consequences at the numerical level, even when considering very small sampling times (Rudolph & Destexhe, 2007).

Furthermore, the computational cost is in theory an order of magnitude better using event-based sampling methods (Brette, 2006), although this may be not always the case in practice (Morrison, Mehring, Geisel, Aertsen, & Diesmann, 2005), as further discussed in this paper.

However, using event-based simulation methods is quite tiresome: Models can be simulated if and only if the next spike-time can be explicitly computed in reasonable time, so that not all models can be used. An event-based simulation kernel is more complicated to use than a clock-based. Existing simulators are essentially clock-based. Some of them integrate event-based as a marginal tool or in mixtures with clock-based methods (Brette et al., 2007). According to this collective review, the only fully supported, scientifically validated, pure event-based simulators is MVASpike (Rochel & Martinez, 2003), the NEURON software proposing a well-defined event-based mechanism (Hines & Carnevale, 2004), while several other implementations (e.g.: DAMMED, MONSTER) exists but are not publicly supported.

In other words, event-based simulation methods may save precision and computation time, but not the scientist time . .

The goal of this paper is to propose solutions to overcome these difficulties, in order to have an easy to use unbiased simulation method.

### **Considering integrate and fire models.**

At the present state of the art, considering adaptive, non-linear, integrate-and-fire model with conductance based synaptic interaction (as e.g. in (Destexhe, 1997; Brette & Gerstner, 2005; Rudolph & Destexhe, 2007)), called punctual conductance based generalized integrate and fire models (gIF), presents several advantages:

- They seem to provide an effective description of the neuronal activity allowing to reproduce several important neuronal regimes, with a good adequacy with respect to biological data, especially in high-conductance states, typical of cortical in-vivo activity (Izhikevich, 2004; Destexhe, Rudolph, & Paré, 2003).
- They provide nevertheless a simplification of Hodgkin-Huxley models, useful both for mathematical analysis and numerical simulations (Gerstner & Kistler, 2002; Izhikevich, 2003).

In addition, though these models have mainly considered one neuron dynamics, they are easy to extend to network structure, including with synaptic plasticity (STDP, Hebbian learning) (Markram, Lübke, Frotscher, & Sakmann, 1997; Pfister & Gerstner, 2006).

However, after a spike, it is always assumed in integrate and fired models that an *instantaneous* reset of the membrane potential occurs. This is a formal simplification, and it has a general spurious effect: the information theory (e.g. the Shannon theorem, stating that the sampling period must be less than half the period corresponding to the highest signal frequency) is not applicable with unbounded frequencies. From the information theoretic point of view, it is a temptation to relate this spurious property to the *erroneous* fact that the neuronal network information is not bounded. In the biological reality, time synchronization is indeed not instantaneous (action potential time-course, synaptic delays, refractoriness, ..). More than that, these biological temporal limits are very precious quantitative elements, allowing to bound and estimate the coding capability of the system.

### What is the paper about

In the first part of this paper, we review review and discuss a few global time constraints and develop their consequences at the modelization level. Section 2 introduces these constraints, section 3 their obvious consequence in terms of the amount of information in a spike train and section 4 discusses in details the impact at the level of the network dynamics, thanks to recent theoretical results.

In the second part of this paper, we develop the consequences of these time constraints at the simulation level. Section 5 shows how event-based simulation of time-constrained networks can be impacted and somehow improved in this context. Section 6 considers punctual conductance based generalized integrate and fire neural network simulation, while section 7 revisits spike-response model simulation within this framework. These mechanisms are experimented in section 8.

Since the contents of this paper requires the reformulation of several well established elements and the integration of data from the literature reused here, we have collected these elements in appendices in order to ease the main text reading while maintaining the self-completeness of the contribution.

## 2 Global time constraints in spike trains

The output of a spiking neural network is a set of events, defined by their occurrence times, up to some precision:

$$\mathcal{F} = \{\dots t_i^n \dots\}, t_i^1 < t_i^2 < \dots < t_i^n < \dots,$$

where  $t_i^n$  corresponds to the  $n$ th spike time of the neuron of index  $i$ , with related inter-spike intervals  $d_i^n = t_i^n - t_i^{n-1}$ . See e.g. (Dayan & Abbott, 2001; Gerstner & Kistler, 2002; Schrauwen, 2007) for an introduction.

In computational or biological contexts, not all multi-time sequences correspond to spike trains since they are constrained by the neural dynamic, while temporal constraints are also to be taken into account: For a single neuron, spike-times are:

- [C1] bounded by a refractory period  $r, r < d_i^{n+1}$ ,
- [C2] defined up to some absolute precision  $\delta t$ , while
- [C3] there is always a minimal delay  $dt$  for one spike to influence another spike, and
- [C4] there is a maximal inter-spike interval  $D$  such that

$$\text{either } d_i^{n+1} < D \text{ or } t_i^{n+1} = +\infty$$

(i.e. either neuron fires within a time delay  $< D$  or it remains quiescent forever).

For biological neurons, orders of magnitude are typically, in milliseconds:

$r$	$\delta t$	$dt$	$D$
1	0.1	$10^{-[1,2]}$	$10^{[3,4]}$

The [C1] constraint is well-known, limiting the maximal rate. See e.g. (Koch, 1999) for an extended discussion on absolute / relative refractory periods.

The [C2] constraint seems obvious but may have several meanings. To define it properly, probabilistic interpretations often consider an additive perturbation, deterministic interpretations may either consider precision

intervals,etc.. Here, we consider that [C2] has the following precise meaning, with respect to synchronization: Two spike-times are not synchronized if separated by more than  $\delta t$ . On the contrary, two spike-trains are synchronized if and only if they repetitively both spike in the same  $\delta t$  time window (Indeed, the fact that two isolated spike-times occur in the same  $\delta t$  time window is not significant). This is a deterministic interpretation and  $\delta t$  can be calculated using 1st order calculus in this context. The [C2] constraint is sometimes “forgotten” in models. In rank coding schemes for instance (Gautrais & Thorpe, 1998) it is claimed that “all” spike-time permutations are significant, which is not realistic since many of these permutations are indistinguishable, because of the bounded precision, as discussed in e.g. (Viéville & Crahay, 2004). Similarly, a few concepts related to “reservoir computing” (e.g. (Maass, 1997)) assume implicitly an unrealistic unbounded time precision. A step further, the  $\delta t$  lower-bound is not made explicit in the litterature (see Appendix A for an evaluation).

Similarly, [C3] is also obvious and allows to avoid any spurious effects<sup>1</sup>, and induce simplifications both at the modelization and simulation level (Morrison et al., 2005). Here we consider  $dt$  including for gap junctions (see Appendix B for bibliographical elements).

The [C4] constraint is less obvious. The idea is that, in the absence of any input (isolated neuron), the potential decreases after a while and the neuron cannot fire anymore. This is true for usual deterministic models, unless a constant input current singular value is choosen. This seems true for cortical neurons, but likely not for all neurons in the brain (see Appendix C for an extended discussion).

As discussed in details in (Cessac & Viéville, 2008) whether the fact [C4] is verified or not, completely changes the nature of the dynamics. In the latter case, a neuron can remain silent a very long period of time, and then suddenly fire, inducing a complete change in the futher state of the system. We distinguish situations with and without [C4] in the sequel.

Considering C[1-3] and optionally [C4], let us now review the related consequences regarding modeling and simulation.

### 3 The maximal amount of information

Considering [C1-2], given a network of spiking neurons observed during a finite period  $[0, T]$ , the number of possible spikes is obviously limited by the refractory period  $r$ . Furthermore, the information contained in all spike times is strictly bounded, since two spike occurrences in a  $\delta t$  window are not distinguishable.

A rather simple reasoning (see Appendix D) yields a rough *upper bound for the amount of information*:

$$N \frac{T}{r} \log_2 \left( \frac{T}{\delta t} \right) \text{ bits during } T \text{ seconds}$$

Taking the numerical values into account it means for large  $T$ , about  $1Kbits/neuron$ .

In fact, the dynamics of a given network constraint very much the the possible spike trains, and the real entropy is lower, when not strongly lower, than this bound.

In the particular case of fast-brain mechanisms where only “the first spike matters” (Thorpe & Fabre-Thorpe, 2001), this amount of information is not related to the permutations between neuron spikes, i.e. of order of  $o(\log(N!)) = N \log(N)$  but simply proportional to  $N$ , in coherence to what is found in (Viéville & Crahay, 2004).

This bound is coherent with results presented in (Rieke, Warland, Steveninck, & Bialek, 1996) considering spike rate and using an information entropy measure. For instance, considering a timing precision of  $0.1 - 1ms$  as set here, the authors obtain an information rate bounded around  $500bits/s$  for a neural receptor.

Note that this is not bad, but good news. For instance, in statistical learning, this corresponds to a coding with large margins, thus as robust as support-vector machines, explaining the surprisingly impressive performances of

---

<sup>1</sup>If a neuron instantaneously fire after receiving a spike, this can generate avalanche effects (another neuron instantaneously fires and so on ..) or even temporal paradoxes (another inhibitory neuron instantaneously fires inhibiting this one, thus not supposed to fire any more).

fast-brain categorization (Viéville & Crahay, 2004).

## 4 Dynamics of time-constrained networks

A step further, taking [C1-3] into account, allows us to “discretize” the spike trains sequences: i.e. use “raster<sup>2</sup>”. The sampling period  $\Delta T$  is taken smaller than  $r$ ,  $\delta t$  and  $dt$ .

In simple models such as basic leaky integrate and fire neuron or integrate and fire neuron models with conductance synapses and constant input current, this discretization allows a full characterization of dynamics. Thus, it has been shown in these two cases that (Cessac, 2008; Cessac & Viéville, 2008):

- [H1] *The raster plot is generically<sup>3</sup> periodic, but, depending on parameters such as external current or synaptic weights, periods can be larger than any accessible computational time;*
- [H2] *There is a one-to-one correspondence between orbits<sup>4</sup> and raster (i.e. raster plots provides a symbolic coding for dynamics).*

The fact [H1] allows to clearly understand to which extends spike trains can code information: Periodic orbits give the code. When the input changes, the orbits are still periodic.

The fact [H2] means that, in these cases, the raster is a “symbolic coding” in the sense that no information is lost by considering spike times and not the membrane potential.

Both facts also allow one to deeply understand the network dynamics: Fig. 1 sketches out some aspects, illustrating the global behavior of the system. Here, attractors are generically stable period orbits.

More precisely, the piece-wise continuous dynamics is locally contracting and after each neuron has fired once is no more dependent on the initial conditions values. When membrane potential is close to the threshold a small perturbation may induce drastic changes in the evolution (otherwise it is damped), this corresponding to a kind of “edge of chaos” (although this differs from the usual notion of chaos in differentiable systems).

### Remarks

Time is discretized, but without any constraint about the “sampling period”. A reasonable order of magnitude for the sampling period is  $dt$  since in the discretized model, a spike is propagated to efferent neurons at least one sampling period later. The [H1] and [H2] results are in fact true at any precision.

In order to understand [H1], it might be important to discuss how “obvious” it is. Time is discretized. If the bounded neuron state (membrane potential) would have been discretized also, we would have a finite state system. In that case, only fixed points and periodic orbits could occur and the result would have been obvious. As a consequence, [H1] reads: even if the neuron state takes continuous values, orbits are still generically periodic.

In a conductance based model, with the additional constraint that conductances depends on previous spikes without a finite horizon, [H1] still holds.

To which extends such a “canonical situation” extends to more complex models is an open question. We can easily conjecture [H1] is a model limitation for all integrate and fire models, defined with an instantaneous reset to a constant value.

<sup>2</sup> Formally, the spike train discretized raster, writes for  $k \geq 0$ :

$$w_i[k] = \#\{t_i^n, k \Delta T \leq t_i^n < (k+1) \Delta T\} \in \{0, 1\}$$

<sup>3</sup> Considering a basic leaky integrate and fire neuron network the result is true except for a negligible set of parameters. Considering an integrate and fire neuron model with conductance synapses the result is true unless the trajectory accumulates on the thresholds.

<sup>4</sup> Here we consider orbits, i.e. infinite trajectories, thus consider the system in its asymptotic stage.

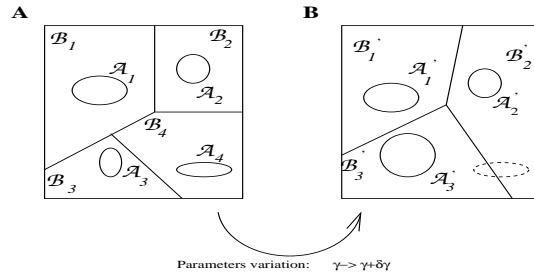


Figure 1: Describing the dynamic landscape of deterministic time-constrained networks. **[A]** The phase space is partitioned into bounded domains  $\mathcal{B}_i$  and for each initial condition in  $\mathcal{B}_i$  the initial trajectory is attracted to an attractor, here not a fixed point, as in, e.g. Hopfield networks, but a periodic orbit  $\mathcal{A}_i$ . **[B]** If the parameters (input, weights) change, the landscape is modified and several phenomena can occur: change in the basins shape, number of attractors, modification of the attractor as for  $\mathcal{A}_3$  in this example; A point belonging to  $\mathcal{A}_i$  in Fig.1 A, can, after modification of the parameters, converge either to attractor  $\mathcal{A}'_2$  or  $\mathcal{A}'_3$ .

However, since the period can be arbitrary large, these models are able to simulate more general models, such as Hodgkin-Huxley (Hodgkin & Huxley, 1952) neuron's assemblies, during a bounded period of time: Periodic orbits approximate chaotic orbits (shadowing lemma). In this sense, they provide useful approximations of biological networks.

The previous conjecture can be explained as follows: Changing the initial value of the membrane potential, one may expect some variability in the evolution. But with the reset, all trajectories collapse on the same point and have obviously the same further evolution. Though this effect can be considered as pathological, it has a great advantage. After reset, the membrane potential evolution does not depend on its past value. This induces an interesting property used in all the Integrate and Fire models that we know: The dynamical evolution is essentially determined by the firing times of the neurons, instead of their membrane potential values.

## 5 Event-based simulation of time-constrained networks.

These theoretical aspects being better understood, let us turn to simulation aspects.

Clock-based and event-based simulations of neural networks make already use at different level of the global time-constraints reviewed here. See e.g. (Brette et al., 2007) for an introduction and a large review and (Rochel & Martinez, 2003; Brette, 2006; Rudolph & Destexhe, 2006; Morrison, Straube, Plesser, & Diesmann, 2007) for simulations with event-based or hybrid mechanisms. However, it appears that existing event-based simulation mechanisms gain at being revisited.

In event-based simulation the exact simulation of networks of units (e.g. neurons) firing events (e.g. spikes) fits in the discrete event system framework (Rochel & Martinez, 2003) and is defined at the neural unit level by :

- 1- the calculation of the next event-time (spike firing),
- 2- the update of the unit when an internal or external event occurs.

At the network level the dual two-stage mechanism, completely implements the simulation:

- a- retrieve the next event-time and the related unit,
- b- update the state of this unit and of efferent units, and update the related event-times,

repeating -a- and -b- while events occur.

Such a strategy is thus based on two key features:

- The calculation of the next event-time, conditioned to the present state and to the fact that no event is received in the meanwhile for each unit;
- The future event-time list, often named priority queue, where the times are sorted in decreasing order and in which event-times are retrieved and updated.

The goal of this section is to revisit these two features considering [C3] and [C4].

Let us consider in this section a network with  $N$  units, an average of  $C$  connections per units, with average rate of events  $M$ .

## 5.1 Event-time queue for time-constrained networks

Although, in the general case, spike-time must be sorted, yielding a  $O(\log(M))$  complexity, there exists data structure allowing to perform retrieve/update operations in constant “ $O(1)$ ” time. Several efficient data structures and algorithms have been proposed to handle such event scheduling task. They are usually based on heap-like structures (Rochel & Martinez, 2003) or sets of buffers associated with some time intervals (such as the calendar queue in (Brette, 2006)). Ring buffers with fixed time step are used in (Morrison et al., 2005).

The basic idea of these structures is to introduce buckets containing event-times in a given time interval. Indexing these buckets allows to access to the related times without considering what is outside the given time interval. However, depending on the fixed or adaptive bucket time intervals, bucket indexing mechanisms and times list managements inside a bucket, retrieve/update performances can highly vary.

Let us now consider [C3] and assume that the bucket time-interval is lower than  $dt$ . If an event in this bucket occurs, there is at least a  $dt$  delay before influencing any other event. Since other events in this bucket occurs in a  $dt$  interval they are going to occur before being influenced by another event. As a consequence, they do not influence each others. They thus can be treated independently. This means that in such a bucket events can be taken into account in any order (assuming that for a given neuron the synaptic effect on incoming spikes can be treated in any order within a  $dt$  window, since they are considered as synchronous at this time-scale).

It thus appears a simple efficient solution to consider a “time histogram” with  $dt$  large buckets, as used in (Morrison et al., 2005) under the name of ring buffer. This optimization is also available in (Rochel & Martinez, 2003) as an option, while (Brette, 2006) uses a standard calendar queue thus more general but a-priori less tuned to such simulation. Several simulation methods take into account [C3] (e.g. (Lee & Farhat, 2001; Connolly, Marian, & Reilly, 2004)).

The drawback of this idea could be that the buffer size might be huge. Let us now consider [C4], i.e. the fact that relative event-time are either infinite (thus not stored in the time queue) or bounded. In this case with  $D = 10^{[3,4]}ms$  (considering fire rate down to  $0.1Hz$ ) and  $10^{-[1,2]}$  (considering gap junctions) the buffer size  $S = D/dt = 10^{5-6}$ , which is easily affordable with computer memories. In other words, thanks to biological order of magnitudes reviewed previously, the histogram mechanism appears to be feasible.

If [C4] does not hold, the data-structure can be easily adapted using a two scales mechanism. A value of  $D$ , such that almost all relative event-time are lower than  $D$  is to be chosen. Almost all event-times are stored in the initial data structure, whereas larger event-times are stored in a transient calendar queue before being reintroduced in the initial data structure. This add-on allows one to easily get rid of [C4] if needed, and still make profit of the initial data structure for almost all events. This is not implemented here, since models considered in the sequel verify [C4].

The fact that we use such a time-histogram and treat the events in a bucket in any order allows us to drastically simplify and speed-up the simulation. Event's retrieve requires less than 5 machine operations and event's update less than 10, including the on-line detection of [C3] or [C4] violation. The simulation kernel<sup>5</sup> is minimal (a 10Kb C++ source code), using a  $\mathcal{O}(D/dt + N)$  buffer size and about  $\mathcal{O}(1 + C + \epsilon/dt) \simeq 10 - 50$  operations/spike ( $> 10^6$  spike/sec on a standard 2.4GHz processor), while  $\epsilon \ll 1$ . In other words, the mechanism is “ $O(1)$ ” as the others, but the time constant is minimal in this case. We save computation time, paying the price in memory.

## Remarks

The fact we use such a time-histogram does not mean we have discretized the event-times. The approximation only concerns the way event are processed. Each event time is stored and retrieved with its full numerical precision. Although [C2] limits the validity of this numerical value, it is indeed important to avoid any additional cumulative round-off. This is crucial in particular to avoid artificial synchrony (Rochel & Martinez, 2003; Morrison et al., 2005).

Using [C3] is not only a “trick”. It changes the kind of network dynamics that can be simulated. For instance, consider a very standard integrate and fire neuron model. It can not be simulated in such a network, since it can instantaneously fire after receiving a spike, whereas in this framework adding an additional delay is required. Furthermore, avalanche phenomena (the fact that neurons instantaneously fire after receiving a spike, instantaneously driven other neurons and so on..) or temporal paradoxes (the fact, e.g., that a inhibitory neuron instantaneously fires inhibiting itself thus . . . is not supposed to fire) can not occur and have not to be taken into account, since we consider the simulation of biological systems, for which [C3] holds.

Only sequential implementation is discussed here. The present data structure is intrinsically sequential. It is however trivial to consider a distributed  $dt$  clock and synchronize several time-histograms on different processors after each bucket has been treated. Furthermore, a time-histogram can distribute the unit next-time and state update calculation on several processors. See also (Mouraud, Puzenat, & Paugam-Moisy, 2005) and (Morrison et al., 2007) for alternatives.

The fact we use such a tiny simulation kernel has several practical advantages. e.g. to use spiking network mechanisms in embedded systems, etc.. However, it is clear this is not “yet another” simulator because a complete simulator requires much more than an event queue (Brette et al., 2007). On the contrary, the implementation has been designed to be used as a plug-in in existing simulators, mainly MVASpike (Rochel & Martinez, 2003).

## 5.2 From next event-time to lower-bound estimation

Let us now consider the following modification in the event-based simulation paradigm. Each unit provides:

- 1- the calculation of *either* the next event-time,  
or the calculation of a lower-bound of the next event-time,
- 2- the update of the neural unit when an internal or external event occurs,  
*with* the indication whether the previously provided next event-time or lower-bound is still valid.

At the network level the mechanism's loop is now:

- a'- retrieve *either* the next event-time and proceed to -b'- or a lower-bound and proceed to -c-
- b'- update the state of this unit and of efferent units, and update the related event-times *only* if required by the unit,
- c- store the event-time lower-bound in order to re-ask the unit at that time.

---

<sup>5</sup>Source code available at <http://enas.gforge.inria.fr>.

A simple way to interpret this modification is to consider that a unit can generate “silent events” which write: “Ask me again at that time, I will better know”.

As soon as each unit is able to *provide the next event-time after a finite number of lower-bound estimations*, the previous process is valid.

This new paradigm is fully compatible with the original, in the sense that units simulated by the original mechanism are obviously simulated here, they simply never return lower-bounds.

It appears that the implementation of this “variant” in the simulation kernel is no more than a few additional line of codes. However, the specifications of an event-unit deeply change, since the underlying calculations can be totally different.

We refer to this modified paradigm as the *lazy* event-based simulation mechanism.

The reason of this change of paradigm is twofold:

- Event-based and clock-based calculations can be easily mixed using the same mechanism.

Units that must be simulated with a clock-based mechanism simply return the next clock-tick as lower-bound, unless they are ready to fire an event. However in this case, each unit can choose its own clock, requires low-rate update when its state is stable or require higher-rate update when in transient stage, etc.. Units with different strategies can be mixed, etc..

For instance, in (Morrison et al., 2005) units corresponding to synapses are calculated in event-based mode, while units corresponding to the neuron body are calculated in clock-based mode, minimizing the overall computation load. They however use a more complicated specific mechanism and introduce approximations on the next spike-time calculations.

At the applicative level, this changes the point of view with respect to the choice of event-based/clock-based simulations. Now, an event-based mechanism can always simulate clock-based mechanisms, using this useful trick.

- Computation time can be saved by postponing some calculations.

Event-based calculation is considered as costless than clock-based calculation because the neuron state is not recalculated at each time-step, only when a new event is input. However, as pointed out by several authors, when a large amount of events arrive to a unit, the next event-time is recalculated a large amount of time which can be much higher than a reasonable clock rate, inducing a fall of performances.

Here this drawback can be limited. When a new event is input the unit needs not to recalculate unless the next event-time is below the last provided event-time bound. This means that if the input event is “inhibitory” (i.e. tends to increase the next event-time) or if the unit is not “hyper-polarized” (i.e. not close to the firing threshold) the calculation can be avoided, while the opportunity to update the unit state again later is to be required instead.

## Remarks

Mixing event-based and clock-based calculations that way is reasonable, only because the event-time queue retrieve/update operations have very low cost. Otherwise, clock-ticks would have generated prohibitory time overloads.

Changing the event-based paradigm is not a simple trick and may require to reconsider the simulation of neural units. This is addressed in the sequel for two important classes of biologically plausible neural units, at the edge of the state of the art and of common use: Synaptic conductance based models (Destexhe, 1997) and spike response models (Gerstner & Kistler, 2002).

## 6 Exact simulation of gIF models

Let us consider a *normalized and reduced* “punctual conductance based generalized integrate and fire” (gIF) neural unit model (Destexhe, 1997) as reviewed in (Rudolph & Destexhe, 2006).

The model is normalized in the sense that variables have been scaled and redundant constant reduced. This is a standard usual one-to-one transformation, reviewed in appendix E for the self-completeness of the paper.

The model is reduced in the sense that both *adaptive* currents and non-linear *ionic* currents are no more explicitly depending on the potential membrane, but on time and previous spikes only. This is a non-standard approximation and a choice of representation carefully discussed in appendix F.

Let  $v$  be the normalized membrane potential and  $\tilde{\omega}_t = \{\dots t_i^n \dots\}$  all spike times  $t_i^n < t$ . Here  $t_i^n$  is the  $n$ -th spike-time of the neuron of index  $i$ . The dynamic of the integrate regime writes:

$$\frac{dv}{dt} + g(t, \tilde{\omega}_t) v = i(t, \tilde{\omega}_t), \quad (1)$$

while the fire regime (spike emission) writes  $v(t) = 1 \Rightarrow v(t^+) = 0$  with a firing threshold at 1 and a reset potential at 0, for a normalized potential.

Equation (1) expands:

$$\frac{dv}{dt} + \frac{1}{\tau_L} [v - E_L] + \sum_j \sum_n r_j (t - t_j^n) [v - E_j] = i_m(\tilde{\omega}_t), \quad (2)$$

where  $\tau_L$  and  $E_L$  are the membrane leak time-constant and reverse potential, while  $r_j()$  and  $E_j$  the spike responses and reverse potentials for excitatory/inhibitory synapses and gap-junctions as made explicit in appendix E. Here,  $i_m()$  is the reduced membrane current, including simplified adaptive and non-linear ionic current.

### 6.1 Derivation of a spike-time lower-bound.

Knowing the membrane potential at time  $t_0$  and the list of spike times arrival, one can obtain the membrane potential at time  $t$ , from (1):

$$v(t) = \nu(t_0, t, \tilde{\omega}_{t_0}) v(t_0) + \int_{t_0}^t \nu(s, t, \tilde{\omega}_{t_0}) i(s, \tilde{\omega}_{t_0}) ds \quad (3)$$

with:

$$\log(\nu(t_0, t_1, \tilde{\omega}_{t_0})) = - \int_{t_0}^{t_1} g(s, \tilde{\omega}_{t_0}) ds \quad (4)$$

Furthermore,

$$\begin{aligned} g(t, \tilde{\omega}_{t_0}) &= \frac{1}{\tau_L} + \sum_j \sum_n r_j (t - t_j^n) &> 0 \\ i(t, \tilde{\omega}_{t_0}) &= \frac{1}{\tau_L} E_L + \sum_j \sum_n r_j (t - t_j^n) E_j + i_m(\tilde{\omega}_{t_0}) &\geq 0 \end{aligned} \quad (5)$$

since the leak time-constant, the conductance spike responses are positive, the reverse potential are positive (i.e. they are greater or equal to the reset potential) and the membrane current is chosen positive.

The spike-response profile schematized in Fig. 2 and a few elementary algebra yields to the following bounds:

$$t \in [t_0, t_1] \Rightarrow r_{\wedge}(t_0, t_1) \leq r(t) \leq r_{\vee}(t_0, t_1) + t r'_{\vee}(t_0, t_1) \quad (6)$$

writing  $r'$  the time derivative of  $r$ , with

$$r_{\wedge}(t_0, t_1) = \min(r(t_0), r(t_1))$$

Here we thus consider a constant lower-bound  $r_{\wedge}$  and a linear or constant upper-bound  $r_{\vee} + t r'_{\vee}$ . The related two parameters are obtained considering in sequence the following cases:

	$t_0 \in$	$t_1 \in$	$r_{\vee}(t_0, t_1)$	$r'_{\vee}(t_0, t_1)$
(i)	$[t_1 - r(t_1)/r'(t_1), t_a]$	$[t_a, t_b]$	$r(t_1) - t_1 r'(t_1)$	$r'(t_1)$
(ii)	$[t_a, t_b]$	$[t_0, +\infty]$	$r(t_0) - t_0 r'(t_0)$	$r'(t_0)$
(iii)	$[t_c, +\infty]$	$[t_0, +\infty]$	$(r(t_0) t_1 - r(t_1) t_0)/(t_1 - t_0)$	$(r(t_1) - r(t_0))/(t_1 - t_0)$
(iv)	$]-\infty, t_1]$	$[t_0, t_b]$	$r(t_1)$	0
(v)	$]-\infty, t_b]$	$[t_b, +\infty]$	$r(t_b)$	0
(vi)	$[t_b, t_1]$	$[t_0, +\infty]$	$r(t_0)$	0

In words, conditions (i) and (ii) correspond to the fact the the convex profile is below its tangent (schematized by  $d$  in Fig. 2), condition (iii) that the profile is concave (schematized by  $d''$  in Fig. 2). In other cases, it can be observed that 1st order (i.e. linear) bounds are not possible. We thus use constant bounds (schematized by  $d'$  in Fig. 2). Conditions (iv) and (vi) correspond to the fact the profile is monotonic, while condition (v) corresponds to the fact the profile is convex. Conditions (iv), (v) and (vi) correspond to all possible cases. Similarly, the constant lower bound corresponds to the fact the profile is either monotonic or convex.

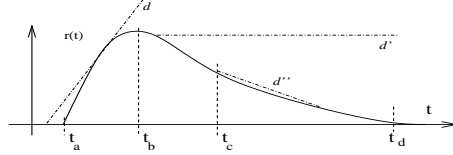


Figure 2: The spike response profile. It has a flat response during the absolute delay interval  $[0, t_a]$ , an increasing convex profile until reaching its maximum at  $t_b$ , followed by a decreasing convex and then concave profile, with an inflexion point at  $t_c$ . After  $t_d$  the response is negligible. See text for details about  $d$ ,  $d'$  and  $d''$ .

From these bounds we derive:

$$\begin{aligned}
 g(t, \tilde{\omega}_{t_0}) &\geq \frac{1}{\tau_{\wedge}(t_0, t_1)} \\
 &\stackrel{\text{def}}{=} \frac{1}{\tau_L} + \sum_j \sum_n r_{j\wedge}(t_0, t_1) \\
 i(t, \tilde{\omega}_{t_0}) &\leq i_{\vee}(t_0, t_1) + t i'_{\vee}(t_0, t_1) \\
 &\stackrel{\text{def}}{=} \left[ \frac{1}{\tau_L} E_L + \sum_j \sum_n r_{j\vee}(t_0, t_1) E_j + i_m(\tilde{\omega}_{t_0}) \right] \\
 &\quad + t \left[ \sum_j \sum_n r'_{j\vee}(t_0, t_1) E_j \right]
 \end{aligned} \tag{7}$$

while  $i'_{\vee}(t_0, t_1) \geq 0$  as the positive sum of  $r'_{j\vee}$  values always positive in our case.

Combining with (3), since values are positive, yields:

$$v(t) \leq v_{\vee}(t) \stackrel{\text{def}}{=} (v(t_0) - v_o) e^{-\frac{t-t_0}{\tau_{\wedge}}} + v_{\bullet} + i_{\bullet} t \tag{8}$$

writing:

$$\begin{aligned}
 i_{\bullet} &\stackrel{\text{def}}{=} \tau_{\wedge}(t_0, t_1) i'_{\vee}(t_0, t_1) \\
 v_{\bullet} &\stackrel{\text{def}}{=} \tau_{\wedge}(t_0, t_1) (i_{\vee}(t_0, t_1) - \tau_{\wedge}(t_0, t_1) i'_{\vee}(t_0, t_1)) \\
 v_o &\stackrel{\text{def}}{=} v_{\bullet} + i_{\bullet} t_0
 \end{aligned} \tag{9}$$

Finally we can solve the equation for  $t^\vee \stackrel{\text{def}}{=} v_\vee^{-1}(1)$  and obtain:

$$t^\vee(t_0, t_1) = \begin{cases} t_0 & , v(t_0) \geq 1 \\ \frac{1-v_\bullet}{i_\bullet} + \tau_\wedge \mathbf{L} \left( \frac{v_\bullet - v(t_0)}{\tau_\wedge i_\bullet} e^{\frac{v_\bullet - 1}{\tau_\wedge i_\bullet}} \right) & , i'_\vee(t_0, t_1) > 0 \\ t_0 + \tau_\wedge \log \left( \frac{v_\bullet - v(t_0)}{v_\bullet - 1} \right) & , i'_\vee(t_0, t_1) = 0, v_\bullet > 1 \\ +\infty & , \text{otherwise} \end{cases} \quad (10)$$

Here  $y = \mathbf{L}(x)$  is the Lambert function defined as the solution, analytic at 0, of  $y e^y = x$  and is easily tabulated.

The derivations details are omitted since they have been easily obtained using a symbolic calculator.

In the case where  $i'_\vee(t_0, t_1) = 0$  thus  $i_\bullet = 0$ ,  $v_\vee(t)$  corresponds to a simple leaky integrate and fire neuron (LIF) dynamics and the method thus consists of upper bounding the gIF dynamics by a LIF in order to estimate a spiking time lower-bound. This occurs when constant upper-bounds is used for the currents. Otherwise (8) and (9) corresponds to more general dynamics.

## 6.2 Event-based iterative solution

Let us apply the previous derivation to calculation of the next spike-time lower-bound for a gIF model, up to a precision  $\epsilon_t$ . One sample run is shown Fig. 3



Figure 3: An example of gIF normalized membrane potential. The trace corresponds to 1s of simulation, the neuron being connected to a periodic excitatory/inhibitory input neuron pair at 100/50 Hz. The weights have been chosen, in order to make the neuron adaptation explicit: the firing frequency decreases until obtaining a sub-threshold membrane potential.

Given a set of spike-times  $t_j^n$  and an interval  $[t_0, t_1]$ , from (7)  $\tau_\wedge$ ,  $i_\vee$  and  $i'_\vee$  are calculated in about  $10^1 MC$  operations. This is the costly part of the calculation<sup>6</sup>, and is equivalent to a single clock-based integration step. Spike response profiles  $r_j()$  and profile derivatives  $r'_j()$  for excitatory/inhibitory synapses and gap junctions are tabulated with a  $\epsilon_t$  step. Then, from (9) and (10) we obtain  $t^\vee(t_0, t_1)$ .

The potential  $v(t_0)$  is calculated using any well-established method, as detailed in, e.g., (Rotter & Diesmann, 1999), and not reviewed here.

The following algorithm guarantees to estimation of a next spike-time lower-bound after  $t_0$ . Let us consider an initial interval of estimation  $d$ , say  $d \simeq 10ms$ :

- a- The lower-bound  $t_\vee = t^\vee(t_0, t_0 + d)$  is calculated.
- b- If  $t_0 + d \leq t_\vee$  the lower-bound value  $t_0 + d$  is returned  
the estimation interval is doubled  $d \leftarrow 2d$

<sup>6</sup>It appears, that since each synapse response corresponds to a linear differential equation which could be analytically integrated, the global synaptic response  $\bar{r}_j(t) = \sum_n r_j(t - t_j^n)$  can be put in closed form, and then bounded by constant values, thus reducing the computation complexity from  $O(MC)$  to  $O(C)$  as detailed in (Rotter & Diesmann, 1999). This well-known issue is not re-addressed here, simply to avoid making derivations too heavy.

- c- If  $t_0 + \epsilon_t < t_v < t_0 + d$  the lower-bound value  $t_v$  is returned  
the estimation interval is reduced  $d \leftarrow 1/\sqrt{2} d$
- d- If  $t_0 < t_v < t_0 + d$ ,  $d \leq \epsilon_t$ , the next spike-time  $t_v$  is returned.

Step -b- corresponds to the case where the neuron is not firing in the estimation interval. Since  $v(t)$  is bounded by  $v_v(t)$  and the latter is reaching the threshold only outside  $[t_0, t_0 + d]$ ,  $t_0 + d$  is a time lower-bound. In addition, a heuristic is introduced, in order to increase the estimation interval in order to save computation steps.

Step -c- corresponds to a strict lower-bound computation, with a relative value higher than the precision  $\epsilon_t$ .

Step -d- assumes that the lower-bound estimation converges towards the true spike-time estimation when  $t_1 \rightarrow t_0$ .

This additional convergence property is easy to derive. Since:

$$\lim_{t_1 \rightarrow t_0} r_{j\wedge}(t_0, t_1) = \lim_{t_1 \rightarrow t_0} r_{j\vee}(t_0, t_1) = r_j(t_0), \lim_{t_1 \rightarrow t_0} r'_{j\wedge}(t_0, t_1) = r'_j(t_0),$$

then:

$$\lim_{t_1 \rightarrow t_0} 1/\tau_\wedge(t_0, t_1) = g(t_0), \lim_{t_1 \rightarrow t_0} i_\wedge(t_0, t_1) = i(t_0), \lim_{t_1 \rightarrow t_0} i'_\wedge(t_0, t_1) = i'(t_0),$$

yielding:

$$\lim_{t_1 \rightarrow t_0} v_v(t) = \bar{v}_v(t) \stackrel{\text{def}}{=} (v(t_0) - \bar{v}_o) e^{-g(t_0)(t-t_0)} + \bar{v}_\bullet + \bar{i}_\bullet t$$

writing:

$$\begin{aligned} \bar{i}_\bullet &\stackrel{\text{def}}{=} 1/g(t_0) i'(t_0) \\ \bar{v}_\bullet &\stackrel{\text{def}}{=} 1/g(t_0) (i(t_0) - 1/g(t_0) i'(t_0)) \\ \bar{v}_o &\stackrel{\text{def}}{=} \bar{v}_\bullet + \bar{i}_\bullet t_0 \end{aligned}$$

We thus obtain a limit expression  $\bar{v}_v$  of  $v_v$  when  $t_1 \rightarrow t_0$ . From this limit expression we easily derive:

$$v(t) - \bar{v}_v(t) = -1/2 g'(t_0) v(t_0) t^2 + O(t^3),$$

and finally obtain a quadratic convergence, with an error closed-form estimation.

The methods thus corresponds to a semi-interval estimation methods of the next spike-time, the precision  $\epsilon_t$  being adjustable at will.

The interval of estimation  $d$  is adjusted by a very simple heuristic, which is of standard use in non-linear numerical calculation adjustment.

The unit calculation corresponds to one step of the iterative estimation, the estimation loop being embedded in the simulator interactions. This is an important property as far as real-time computation is concerned, since a minimal amount of calculation is produced to answer as soon as possible at a minimal question.

This “lazy” evaluation method is to be completed by other heuristics:

- if the input spike is inhibitory thus only delaying the next spike-time, re-calculation can be avoided;
- if all excitatory contributions  $g_v = M r^+(t_b)$  are below the spiking threshold, spike-time is obviously infinity;
- after a spike the refractory period allows to postpone all calculation (although synaptic conductances still integrate incoming spikes);
- etc.. which are not going to further detailed here since well-known.

In any case, comparing to other gIF models event-based simulation methods (Brette, 2006, 2007; Rudolph & Destexhe, 2006), this alternative method allows one to control the spike-time precision, does not constraint the synaptic response profile and seems of rather low computational cost, due to the “lazy” evaluation mechanisms.

## 7 About event-based simulation of SRM models

Among spiking-neuron models, the Gerstner and Kistler spike response model (SRM) (Gerstner & Kistler, 2002) of a biological neuron defines the state of a neuron via a single variable:

$$u_i(t) = r_i i(t) + \nu_i(t - t_i^*) + \sum_j \sum_{t_j^n \in \mathcal{F}_j} w_{ij} \varepsilon_{ij}(t - t_i^*, (t - t_j^n) - \delta_{ij}) \quad (11)$$

where  $u_i$  is the neuron state related to the membrane potential,  $i$  is the continuous input current for an input resistance  $r_i$ . The neuron fires when  $u_i(t) \geq \theta_i$ , for a given threshold,  $\nu_i$  describes the neuronal response to its own spike (neuronal refractoriness),  $t_i^*$  is the last spiking time of the  $i$ th neuron,  $\varepsilon_{ij}$  is the neuronal response to pre-synaptic spikes at time  $t_j^n$  post-synaptic potential (see Fig. 4),  $w_{ij}$  is the *connection strength* (excitatory if  $w_{ij} > 0$  or inhibitory if  $w_{ij} < 0$ ) and  $\delta_{ij}$  is the *adaptive delay* (including axonal delay).



Figure 4: Potential profiles used in equation (11). The original exponential profiles derived by the authors of the model are shown as thin curves and the piece-wise linear approximation as thick lines.

This model is very useful both at the theoretical and simulation levels. At a computational level, it has been shown (see (Maass & Bishop, 2003) for a review) with this model, considering piece-wise linear approximations of the potential profiles (ISRM), that any feed-forward or recurrent (multi-layer) analog neuronal network (à-la Hopfield, e.g., McCulloch-Pitts) can be simulated arbitrarily closely by an insignificantly larger network of spiking neurons with analog inputs and outputs encoded by temporal delays of spikes (even in the presence of noise) (Maass, 1997; Maass & Natschlager, 1997). Note that the reverse is not true, spiking networks being computationally more efficient than analog networks. These results highly motivate the use of spiking neural networks.

This model has also been used to implement computation with spikes (see e.g. (Schrauwen, 2007) for a review), including high-level specifications of neural network processing related to variational approaches (Viéville, Chemla, & Kornprobst, 2007), using spiking networks (Viéville & Rochel, 2006). The authors used again a ISRM to implement their non-linear computations in closed-forms. Let us make explicit here the fact a ISRM can be simulated on an event-based simulator for two simple reasons:

- the membrane potential is a piece-wise linear function as the sum of piece-wise linear functions (as soon as the optional input current is also piece-wise constant or linear),
- the next spike-time calculation  $t^{n+1} = \arg \min_t, u_i(t) = 1$  is obvious to calculate on a piece-wise linear potential profile, scanning the linear segments and detecting the 1st intersection with  $u = 1$  if any. The related piece-wise linear curve data-structure has been implemented<sup>5</sup> and support three main operations: - At each spike occurrence, add linear pieces to the curve corresponding to refractoriness or synaptic response. - Reset the curve, after a spike occurrence and also to clean-up past data. - Solve the next spike-time calculation. This is illustrated in Fig. 5.

This is to be compared with other simulations (e.g. (Mattia & Giudice, 2000; Ruf, 1998)) where stronger simplifications of the SRM models have been introduced to obtain a similar efficiency, whereas other authors propose heavy numerical resolutions at each step. When switching from piece-wise linear profiles to the original exponential profiles (Gerstner & Kistler, 2002), the equation to solve is now of the formal form:

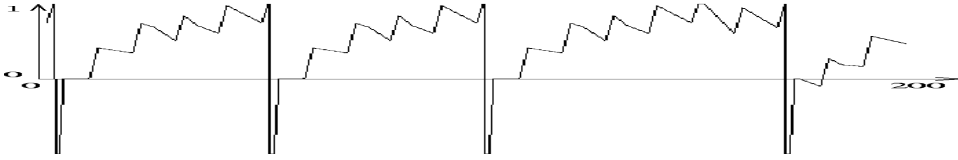


Figure 5: An example of ISRM normalized membrane potential. The trace corresponds to 200ms of simulation, the neuron being defined by biologically plausible parameters ad reviewed in appendix E and connected to a periodic excitatory/inhibitory input neuron pair, as in Fig. 3.

$$1 = \sum_{i=1}^n \lambda_i e^{t/\tau_i},$$

without any closed-form solution as soon as  $n > 1$ . One elegant solution (Brette, 2007) is to approximate the time-constant by rational numbers and reduce this problem to a polynomial root finding problem. Another solution is to upper-bound the exponential profiles by piece-wise linear profiles in order to obtain a lower-bound estimation of the next spike-time and refine in the same way as what has been proposed in the previous section. Since the mechanism is identical, we are not going to further develop.

In any case, this very powerful phenomenological model of a biological dynamics, can be simulated with several event-based methods, including at a fine degree of precision, using more complex piece-linear profiles.

## 8 Experimental benchmarks

In order to validate this idea, we have reproduced the benchmark proposed in (Brette et al., 2007) which is dedicated to event-based simulation: it consists of 4000 IF neurons, which 80/20% of excitatory/inhibitory neurons, connected randomly using a connection probability of  $1/32 \simeq 3\%$ . So called “voltage-jump” synaptic interactions are used: the membrane potential is abruptly increased/decreased by a value of  $0.25/2.25mV$  for each excitatory/inhibitory event. Here, we also introduce a synaptic delay of  $2/4ms$  respectively and an absolute refractory period of  $1ms$ , both delays being corrupted by an additive random noise of  $10\mu s$  of magnitude. We also have increased the network size and decreased the connection probability to study the related performances. In this network a synapse is simply defined by an index, weights are constant. See (Brette et al., 2007) for further details.

In term of performances, on a standard portable computer (Pentium M 750 1.86 GHz, 512Mo of memory) we process about  $10^{6-7}$  spike-time updates / second, given the network size and connectivity. Performances reported in Table 1 confirm that the algorithmic complexity only marginally depends on the network size, while it is mainly function of the number of synapses. We also notice the expected tiny overhead when iterating on empty boxes in the histogram, mainly visible when the number of spike is small. This overhead is constant for a given simulation time and. In a nutshell this methods allows about  $10^{6-7}$  updates (spike-time insertion/deletion) pro second. The lack of proportionality in performances is due to the introduction of some optimization in the evaluation of spike-times, which are not updated if unchanged. We also have tested the performances using randomly spiking neurons and several other set of parameters have been used, not reported in Table 1, since they simply corroborate the explained results.

A step further, we also made profit of the present event-based kernel which is compatible with clock-based benchmarks. We reproduced benchmarks close to what is proposed in (Brette et al., 2007) with current-based interactions (CUBA model) and another one with conductance-based interactions (COBA model). In our context, current based interactions correspond to gap junctions, while conductance-based interactions correspond to synaptic junctions. However, in the COBA original models, when a spike occurs, the synaptic conductance is

Network size	Number of synapses	Number of $10^6$ updates/second	$D$	$dt$
$2^{12}$	$\simeq 2^{19}$	14	0.1s	1 $\mu$ s
$2^{13}$	$\simeq 2^{21}$	12	0.1s	1 $\mu$ s
$2^{14}$	$\simeq 2^{23}$	8	0.1s	1 $\mu$ s
$2^{15}$	$\simeq 2^{25}$	6	0.1s	1 $\mu$ s
$2^{16}$	$\simeq 2^{26}$	5	0.1s	1 $\mu$ s
$2^{16}$	$\simeq 2^{25}$	5	0.1s	1 $\mu$ s
$2^{16}$	$\simeq 2^{24}$	5	0.1s	1 $\mu$ s
$2^{13}$	$\simeq 2^{21}$	11	1s	1 $\mu$ s
$2^{13}$	$\simeq 2^{21}$	12	1s	10 $\mu$ s
$2^{13}$	$\simeq 2^{21}$	12	0.1s	10 $\mu$ s

Table 1: Simulation performances, for  $10^5$  spike firings and about 0.1s of simulation time. The CPU time is about 2s for  $2^{13}$  and  $2^{21}$  and does not depend on  $D$  or  $dt$  values, as expected. The network size and number of synapses (via the connection probability) is varied. The performance is mainly function of the number of synapses, not the number of neurons. The spike-time structure upper and lower bounds  $D$  and  $dt$  have only a marginal influence on the performances, see text for details.

instantaneously incremented by a quantum value (6 nS and 67 nS for excitatory and inhibitory synapses, respectively) and decayed exponentially with a time constant of 5 ms and 10 ms for excitation and inhibition, respectively, whereas here an “alpha” profile is used. In CUBA models, the conductance quanta is of 0.27 nS and 4.5 nS for excitatory and inhibitory synapses, respectively. Despite the use of “exponential” profiles instead of “alpha” profiles and a few numerical approximations at the implementation level, we have obtained similar results as illustrated in Fig. 6, as reported in (Brette et al., 2007).

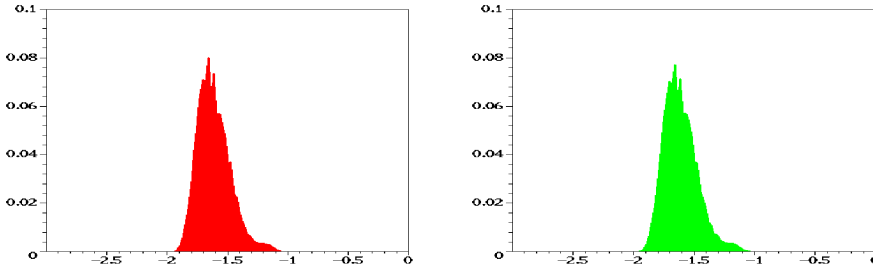


Figure 6: Inter-spike interval histogram for excitatory neurons (in red) and inhibitory neurons (in green). The abscissa is the decimal log of the interval and the ordinate the inter-spike observed probability. Results qualitatively corresponds to the expected result for this kind of benchmark, with a distribution from 10ms to more than 100ms with a peak around 50ms similar for both excitatory and inhibitory neurons. Here, there are inter-spike intervals higher than 100ms up to 1s but only with a residual quantity.

Finally, the result of a simulation with the default parameters proposed in appendix E and F is proposed in Fig. 7 to qualitatively verify the related network dynamics.

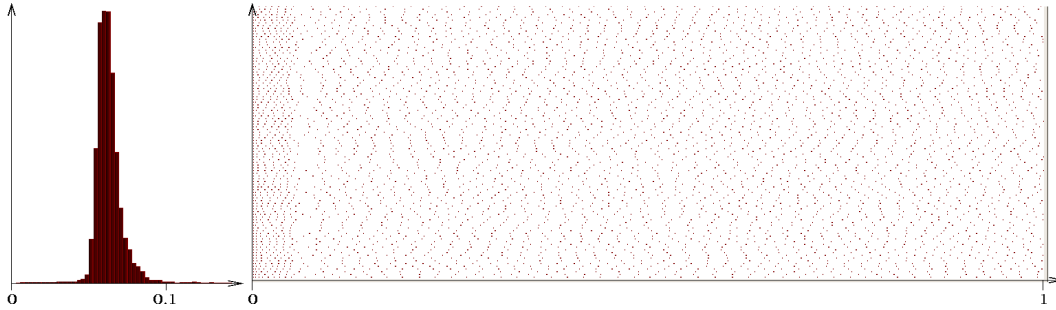


Figure 7: Inter-spike interval histogram (left view) in linear coordinates measured after  $t > 0.1s$ . Raster plot (right-view) during 1s of simulations.

## 9 Conclusion

Taking global temporal constraints into account, it has been possible to better understand at both the modelization and simulation levels to which extends spiking mechanisms are bounded and simplified in such a context. It appears that although obvious, consequences of these bounds may be skipped in some approaches.

In models such as basic leaky integrate and fire neuron or integrate and fire neuron models with conductance synapses and constant input current, this allows a full characterization of dynamics (Cessac, 2008; Cessac & Viéville, 2008), corresponding in this context to periodic orbits with a one-to-one correspondence between spike-trains and membrane potential. At the simulation level, this corroborates the fact that challenge is to generate spike-trains corresponding to what is observed in the biology or to what is required for computational processing, without the necessity to precisely reproduce the internal neural state. This is a very important simplification when the goal is to switch from the neural scale to the network one.

At a much more practical level, event-based simulation of spiking network is somehow improved in this context: the underlying data-structures are strongly simplified, while event-based and clock-based mechanisms can be easily mixed. These ideas are applied to rather complicated models such as punctual conductance based generalized integrate and fire neural network simulation, or spike-response model simulation. Such improvement can be used as a plug-in in existing simulators, such as MVASpike (Rochel & Martinez, 2003).

As far as computational mechanisms are concerned, the key point here is that it becomes easier to mix spiking mechanisms with other processing mode and to mix spiking mechanisms at the unit level and other analog or event-based mechanisms at higher scales. Having event-based spiking mechanisms “simplified”, we now can study how to integrate them at the level of a cortical map, which is the next step on this track.

## A Spike time precision evaluation

Considering that the spike-time of a real neuron is defined by the membrane potential maxima  $V(t_i)$  at time  $t_i$ , we obtain around  $t_i$ , assuming differentiability of  $V$ :

$$V(t) = V(t_i) + \kappa(t - t_i)^2 + o(|t - t_i|^3),$$

with  $\kappa = d^2V/dt^2(t_i)$  and easily derive, as a rule of thumb for the spike-time precision  $\delta t$ :

$$\delta t \simeq \sqrt{\frac{\langle \delta V \rangle}{\langle \kappa \rangle}}.$$

where the average  $\langle \rangle$  is to be taken over a set of measurements. This formula is derived from standard 1st order

error analysis.

In order to roughly estimate spike-time precision, we have taken a few dozen of spike profiles in several spike trains (Carandini & Ferster, 2000; Koch, 1999) and graphically estimates the values on a zoom of the provided figures. We have obtained  $\delta t \simeq 0.1ms$ , with a peak curvature order of magnitude of  $\langle \kappa \rangle = 100mV/ms^2$  as illustrated in Fig. 8, considering a voltage precision of  $\langle \delta V \rangle = 10\mu V$ , i.e. at the order of magnitude of the membrane potential noise (Koch, 1999). Similar numerical values are obtained reading other electro-physiological data (Carandini & Ferster, 2000).

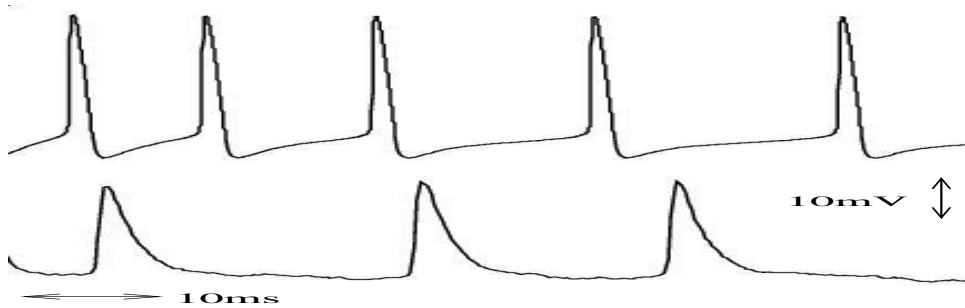


Figure 8: Two examples of spike profiles in the cat primary visual cortex. The peak curvature order of magnitude are  $30 - 100mV/ms^2$ .

Furthermore, similar order of magnitude is obtained in the literature, considering the numerical precision in inter-neuron synchronization (Crook, Ermentrout, & Bower, 1998) which is found of about  $1ms$ , while (Mainen & Sejnowski, 1995) (e.g. in Fig.2B) report submillisecond accuracy *in vitro*, but no higher than  $0.1ms$ .

## B Spike time propagation evaluation

The smaller delays (Koch, 1999; Burnod, 1993) involving the pre-synaptic axonal delay, synaptic delay and post-synaptic dendritic delay seems to be at least of  $0.5ms$ , with delay up to  $10ms$  for inter cortical maps transmissions. A step further, many local inter-neuronal connections in the cortex are realized through electrical gap junctions (Galarreta & Hestrin, 2001), this being predominant between cells of the same sub-population (Amitai et al., 2002). In such a case the inter-neuron delays are much smaller, but still measurable, since the transmission is mainly due to the spike potential raise, whose time constant is about  $0.1 - 0.2ms$  (see (Lewis & Rinzel, 2003) for a discussion about the electrical transmission in this case). It is thus a reasonable assumption to consider that local electrical connections are delayed by  $dt \gtrsim 0.1ms$ .

Gap junctions delays are much smaller ( $dt \gtrsim 10\mu s$ ) but still non negligible (Lewis & Rinzel, 2003; Koch, 1999).

## C Spike time upper-bound evaluation

At the simulation level, [C4] is easily violated for deterministic neural model with constant current input, able to integrate during a unbounded period of time, or with maintained sub-threshold oscillations. But this singular condition is easy to check and to avoid, and a maximal spontaneous firing period can be derived. Synaptic conductance based models (Destexhe, 1997) and spike response models (Gerstner & Kistler, 2002) usually omit this constant

current and their intrinsic “leak” guaranty that [C4] is not violated. On the contrary, with stochastic models, [C4] is to be reconsidered, since there is always a “chance” to fire a spike, with a decreasing probability as time increases.

At the biological level<sup>7</sup>, in vitro, a cortical pyramidal regular spiking type neuron without synaptic input remains silent since its membrane potential is close to the resting potential (Koch, 1999). In vivo, in the cortex, current observations show that a neuron is always firing (Dayan & Abbott, 2001) (unless it is dead). This is due the large amount of neuromodulators, inducing depolarization and a membrane potential close to the firing threshold. However, this differs from [C4], where isolated neurons are considered. On the contrary, thalamic neurons can spontaneous fire after a long rest period (Par, Bouhassira, Oakson, & Datta, 1990). Even in vitro, their internal currents such as IT (low threshold transient Ca2+ current) or IH (hyper-polarization-activated cation current) can induce spikes (due to oscillatory behaviors) (McCormick & Bal, 1997).

## D Information upper bound derivation

Let us consider the first spike time  $t_j^1$ , this spike being fired by, say, the neuron of index  $j$ . A single neuron, (i) either fires not later than  $t_j^1 + \delta t$  thus at a time not distinguishable from  $t_j^1$  by an observer, or (ii) fires at least  $\delta t$  later. In order to be meaningful these first spikes must occur in distinct temporal boxes of width  $\delta t$ , the precise location of the box being fixed by the first time occurrence, as schematized in Fig. 9. Since there is a refractory period of  $r > \delta t$  the second and next spikes will never be mixed with their predecessor but are going to be subject to the same limitation.

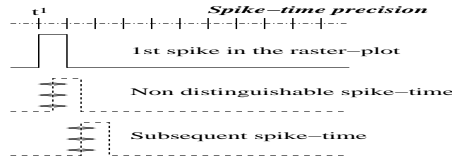


Figure 9: Evaluating the information in a set of spike times. See text for details.

As a consequence, in average, not more than introducing for each neuron spikes every  $r$  seconds in a temporal histogram with  $\delta t$  width temporal boxes can be done, as illustrated if Fig. 9. For each neuron, in  $[0, T]$ , there are  $T/\delta t$  choices for the first spike, less than  $T/\delta t - 1$  for the second etc.. This means that for the  $T/r$  maximal number of spikes, they are less than  $(T/\delta t)^{T/r}$  choices. Assuming, in the maximal case, that each neuron is independent, we obtain the proposed bound.

## E About gIF model normalization

Let us review how to derive an equation of the form of (2). We follow (Izhikevich, 2004; Brette & Gerstner, 2005; Rudolph & Destexhe, 2006) in this section. We consider here a voltage dynamics of the form:

$$\frac{dV}{dt} + I^{leak} + I^{syn} + I^{gap} = I^{ext} + I^{adp} + I^{ion}$$

thus with leak, synaptic, gap-junction, external currents discussed in this section, while adaptive and ionic currents are discussed in the next section.

<sup>7</sup>We are especially thankful to Dr. Thierry Bal, for a scientific discussion on this subject.

## Membrane voltage range and passive properties

The membrane potential, outside spiking events, verifies:

$$V(t) \in [V_{\text{reset}}, V_{\text{threshold}}]$$

with typically  $V_{\text{reset}} \simeq E_L \simeq -80mV$  and a threshold value  $V_{\text{threshold}} \simeq -50mV \pm 10mV$  as illustrated in Fig. 10.

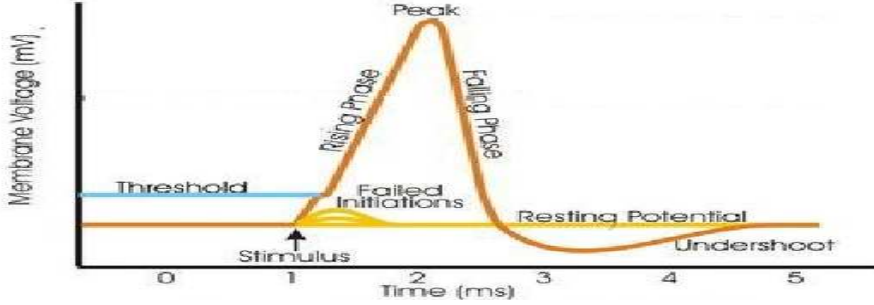


Figure 10: A schematic view of the membrane potential. Between two action potentials, i.e. spikes, the potential is between its “reset” and “threshold” value. When the threshold is reached an action potential of about 1-2 ms is issued and followed by refractory period of 2-4 ms (more precisely, an absolute refractory period of 1-2 ms without any possibility of another spike occurrence followed by a relative refraction to other firing). Voltage peaks are at about  $40mV$  and voltage undershoots about  $-90mV$ . The threshold is in fact not sharply defined, as discussed in the text.

The reset value is typically fixed, whereas the firing threshold is inversely related to the rate of rise of the action potential upstroke (Azouz & Gray, 2000). Here it is taken as constant. This adaptive threshold diverging mechanism can be represented by a non-linear ionic current (Izhikevich, 2004; Brette & Gerstner, 2005), as discussed in Appendix F.

From now on, we renormalize each voltage between  $[0, 1]$  writing:

$$v = \frac{V - V_{\text{reset}}}{V_{\text{threshold}} - V_{\text{reset}}} \quad (12)$$

The membrane leak time constant  $\tau_L \simeq 20ms$  is defined for a reversal potential  $E_L \simeq -80mV$ , as made explicit in (2).

The membrane capacity  $C = SC_L \simeq 300pF$ , where  $C_L \simeq 1\mu Fcm^{-2}$  and the membrane area  $S \simeq 38.013\mu m^2$ , is integrated in the membrane time constant  $\tau_L = C_L/G_L$  where  $G_L \simeq 0.0452mScm^{-2}$  is the membrane passive conductance.

From now on, we renormalize each current and conductance divided by the membrane capacity. Normalized conductance units are  $s^{-1}$  and normalised current units  $V/s$ .

## Synaptic currents

In conductance based model the occurrence of a post synaptic potential on a synapse results in a change of the conductance of the neuron. Consequently, it generates a current of the form:

$$I^{syn}(V, t) = \sum_j G_j^+(t, \tilde{\omega}_t) [V(t) - E_+] + \sum_j G_j^-(t, \tilde{\omega}_t) [V(t) - E_-],$$

for excitatory + and inhibitory – synapses, where conductances are positive and depend on previous spike-times  $\tilde{\omega}_t$ .

In the absence of spike, the synaptic conductance vanishes (Koch, 1999), and spikes are considered having an additive effect:

$$G_j^\pm(t, \tilde{\omega}_t) = \bar{G}^\pm \sum_n r^\pm(t - t_j^n)$$

while the conductance time-course  $r^\pm(t - t_j^n)$  is usually modelled as an “exponential”, “alpha” (see Fig. 11) or two-states kinetic (see Fig. 12) profile, where  $H$  is the Heaviside function (related to causality).

Note, that the conductances may depend on the *whole past history* of the network, via  $\tilde{\omega}_t$ .

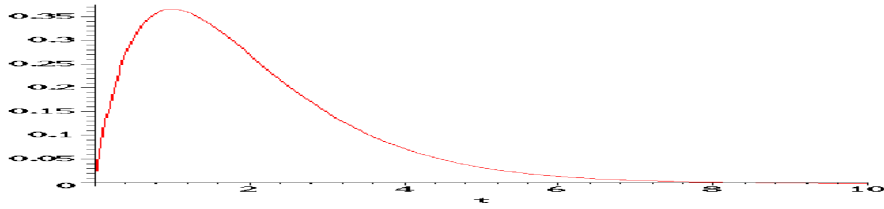


Figure 11: The “alpha” profile  $\alpha(t) = H(t) \frac{t}{\tau} e^{-\frac{t}{\tau}}$  plotted here for  $\tau = 1$ . It is maximal at  $t = \tau$  with  $\alpha(\tau) = 1/e$ , the slope at the origin is  $1/\tau$  and its integral value  $\int_0^{+\infty} \alpha(s) ds = \tau$  since  $(\int \alpha)(t) = (\tau - t) e^{-\frac{t}{\tau}} + k$ . This profile is concave for  $t \in ]0, 2\tau[$  and convex for  $t \in ]2\tau, +\infty[$ , while  $\alpha(2\tau) = 2/e^2$  at the inflexion point.

The “exponential” profile ( $r(t) = H(t) e^{-\frac{t}{\tau}}$ ) introduces a potentially spurious discontinuity at the origin. The “beta” profile is closer than the “alpha” profile to what is obtained from a bio-chemical model of a synapse. However, it is not clear whether the introduction of this additional degree of freedom is significant here. Anyway, any of these can be used for simulation with the proposed method, since their properties correspond to what is stated in Fig. 2.

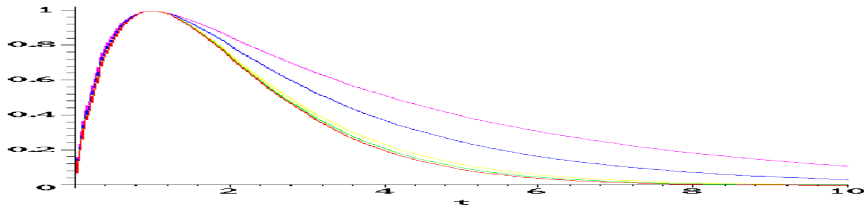


Figure 12: The two-states kinetic or “beta” profile  $\beta(t) = H(t) \frac{1}{\kappa-1} (e^{-\frac{t}{\tau}} - e^{-\kappa \frac{t}{\tau}})$  is plotted with a normalized magnitude for the same  $\tau = 1$  as the “alpha” profile but different  $\kappa = 1.1, 1.5, 2, 5, 10$  showing the effect of this additional degree of freedom, while  $\lim_{\kappa \rightarrow 1} \beta(t) = \alpha(t)$ . The slope at the origin and the profile maximum can be adjusted independently with “beta” profiles. It is maximal at  $t_\bullet = \tau \ln(\kappa)/(\kappa - 1)$  the slope at the origin is  $1/\tau$  and its integral value  $\tau/\kappa$ . The profile is concave for  $t \in ]0, 2t_\bullet[$  and convex for  $t \in ]2t_\bullet, +\infty[$ .

There are typically, in real neural networks,  $10^4$  excitatory and about  $2 \cdot 10^3$  inhibitory synapses. The corresponding reversal potential are  $E_+ \simeq 0 \text{ mV}$  and  $E_- \simeq -75 \text{ mV}$ , usually related to AMPA and GABA receptors. In average:  $\bar{G}_j^+ \simeq 0.66 \text{ nS}$ ,  $\tau^+ \simeq 2 \text{ ms}$  and  $\bar{G}_j^- \simeq 0.63 \text{ nS}$ ,  $\tau^- \simeq 10 \text{ ms}$ , for excitatory and inhibitory synapses

respectively, thus about  $570ms^{-1}$ ,  $600ms^{-1}$  in normalized units, respectively. The coefficients  $\bar{G}^{\pm}$  give a measure of the synaptic strength (unit of charge) and vary from one synapse to another and are also subject to adaptation.

This framework affords straightforward extensions involving synaptic plasticity (e.g. STDP, adjusting the synaptic strength), not discussed here.

### Gap junctions

It has been recently shown, that many local inter-neuronal connections in the cortex are realized though electrical gap junctions (Galarreta & Hestrin, 2001), this being predominant between cells of the same sub-population (Amitai et al., 2002). At a functional level they seem to have an important influence on the synchronicity between the neuron spikes (Lewis & Rinzel, 2003). Such junctions are also important in the retina (Wohrer & Kornprobst, 2008).

The electrotonic effect of both the sub-threshold and supra-threshold portion of the membrane potential  $V_j(t)$  of the pre-junction neuron of index  $j$  seems an important component of the electrical coupling. This writes (Wohrer & Kornprobst, 2008; Lewis & Rinzel, 2003):

$$I^{gap}(V, t) = \sum_j G_j^* [V_j(t) - V(t)] + E_{\bullet} \sum_n r(t - t_j^n)$$

where  $G_j^*$  is the electrical coupling conductance, the term  $V_j(t) - V(t)$  accounts for the sub-threshold electrical influence while and  $E_{\bullet}$  parameterizes the spike supra-threshold voltage influence.

Regarding the supra-threshold influence, a value  $E_{\bullet} \simeq 80mV$  corresponds to the usual spike voltage magnitude of the spiking threshold, while  $\tau_{\bullet} \simeq 1ms$  corresponds to the spike raise time. Here  $r()$  profile accounts for the action potential itself, slightly filtered by the biological media, while the gap junction intrinsic delay is of about  $10\mu s$ . These choices seem reasonable with respect to biological data (Galarreta & Hestrin, 2001; Lewis & Rinzel, 2003)

A step further, we propose to neglect the sub-threshold term for three main reasons. On one hand, obviously the supra-threshold mechanism has a higher magnitude than the sub-threshold mechanism, since related to action potentials. Furthermore, because of the media diffusion, slower mechanisms are smoothed by the diffusion, whereas faster mechanisms better propagate. On the other hand, this electrical influence remains local (quadratic decrease with the distance) and is predominant between cells of the same sub-population which are either synchronized or have a similar behavior, as a consequence  $|V_j(t) - V(t)|$  remains small for cells with non-negligible electrical coupling. Furthermore, a careful analysis of such electrical coupling (Lewis & Rinzel, 2003) clearly shows that the sub-threshold part of the contribution has not an antagonist effect on the neuron synchrony, i.e., it could be omitted without changing qualitatively the gap junction function.

As a conclusion, we are able to take gap junction into account with a minimal increase of complexity, since we obtain a form similar to synaptic currents, using very different parameters

### External currents

Direct input (or external) current is often related to electro-physiological clamps. At another level of representation, the average activity of the neuron can be modeled by a constant or random input current. In both cases, the way the proposed simulation methods is proposed requires to assume such external current to be taken as constant between two spikes, i.e. having temporal variations small enough to be neglected. If not, it is easy to associate to the external current an event unit which fires at each new current value, in order the neuron to take this new value into account.

## F About gIF model reduction

Let us now discuss choices of modelization for  $I_m = I^{adapt} + I^{ionic}$

### Adaptive current

The Fitzhugh-Nagumo reduction of the original Hodgkin-Huxley model (Hodgkin & Huxley, 1952) represents the average kinematics of the membrane channels by an adaptive current. Its dynamics is defined, between two spikes, by a second equation of the form:

$$\tau_w \frac{dI^{adapt}}{dt} = g_w (V - E_L) - I^{adapt} + \Delta_w \delta (V - V_{\text{threshold}}),$$

with a slow time-constant adaptation  $\tau_w \simeq 144ms$ , a sub-threshold equivalent conductance  $g_w \simeq 4nS$  and a level  $\Delta_w \simeq 0.008nA$  of spike-triggered adaptation current. It has been shown (Izhikevich, 2003) that when a model with a quadratic non-linear response is increased by this adaptation current, it can be tuned to reproduce qualitatively all major classes of neuronal in-vitro electro-physiologically defined regimes.

Since the time-constant adaptation is slow, and since the past dependence in the exact membrane potential value is removed when resetting, we may neglect the coupling with  $V$  for short periods of time. This writes:

$$\begin{aligned} I^{adapt}(V, t) &\simeq e^{-\frac{(t-t_0)}{\tau_w}} I^{adapt}(t_0) + \frac{g_w}{\tau_w} \int_{t_0}^t e^{-\frac{(t-s)}{\tau_w}} (V(s) - E_L) ds + \Delta_w \#(t_0, t) \\ &\simeq \underbrace{e^{-\frac{(t-t_0)}{\tau_w}} I^{adapt}(t_0) + g_w \left(1 - e^{-\frac{(t-t_0)}{\tau_w}}\right) (\bar{V} - E_L)}_{\text{slow variation}} + \underbrace{\Delta_w \#(t_0, t)}_{\text{spike-time dependent}} \end{aligned}$$

where  $\#(t_0, t)$  is the number of spikes in the  $[t_0, t]$  interval while  $\bar{V}$  is the average value between  $t$  and  $t_0$ , the previous spike-time.

This adaptive term is mainly governed by the spike-triggered adaptation current, the other part of the adaptive current being a standard leak. This is also verified, by considering the linear part of the differential system of two equations in  $V$  and  $I^{adapt}$ , for an average value of the conductance  $\bar{G}^+ \simeq 0.3 \dots 1.5nS$  and  $\bar{G}^- \simeq 0.6 \dots 2.5nS$ . It appears that the solutions are defined by two decreasing exponential profiles with  $\tau_1 \simeq 16ms \ll \tau_2 \simeq 115ms$  time-constants, the former being very close to the membrane leak time-constant and the latter inducing very slow variations.

In other words *current adaptation is, in this context, mainly due to spike occurrences* and the adaptive current is no more directly a function of the membrane potential but function of the spikes only.

For correctness of the approximation, we have to constraint the adaptive current in order the global current to remain positive.

### Non-linear ionic currents

Let us now consider the non-linear active (mainly Sodium and Potassium) currents responsible for the spike generation. In models designed to simplify the complex structure of Hodgkin-Huxley equations, the sub-threshold membrane potential is defined by a supra-linear kinematics, taken as e.g. quadratic or exponential, the latter form closer to observed biological data (Brette & Gerstner, 2005). It writes, for example:

$$I^{ion}(V) = \frac{C \delta_a}{\tau_L} e^{\frac{V-E_a}{\delta_a}} \geq 0 \text{ with } \left. \frac{dI^{ion}}{dV} \right|_{V=E_a} = \frac{C}{\tau_L} \quad (13)$$

with  $E_a \simeq -40mV$  the threshold membrane state at which the slope of the I-V curve vanishes, while  $\delta_a = 2mV$  is the slope factor which determines the sharpness of the threshold. There is no need to define a precise threshold in this case, since the neuron fires when the potential diverges to infinity.

A recent contribution (Touboul, 2008) re-analyzes such non-linear currents, proposes an original form of the ionic current, with an important sub-threshold characteristic not present in previous models (Izhikevich, 2003; Brette & Gerstner, 2005) and show that we obtain the correct dynamics providing that the profile is mainly non-negative and strictly convex, not necessarily a quadratic or exponential function.

Making profit of this general remark, we propose to use a profile of the form of (13), but simply freeze the value of  $V$  to the the previous value obtained at the last spike time occurrence. This allows us to consider a supra-linear profile which depends only on the previous spike times. This approximation may slightly underestimate the ionic current before a spike, since  $V$  is increasing with time. However, when many spikes are input, as it is the case for cortical neurons, errors are minimized since the ionic current update is made at high rate.

At a phenomenological level (Izhikevich, 2003) the real goal of this non-linear current in synergy with adaptive currents is to provide several firing regimes. Let us verify experimentally that even coarser approximations allow to attain this goal.

## Experimenting reduced adaptive and ionic currents

In order to experiment about the two previous points, we consider a very simple model whose evolution equation at time  $t$  for the membrane potential  $v$  is:

$$\begin{aligned}
 & \text{if } (t = 0) && v = 0; u = 0; t_{-0} = 0; \\
 & \text{else if } (v \geq 1) && v = 0; u = u + k; t_{-0} = t; \\
 & \text{else} && \dot{v} = -g(v - E) - u + i; \\
 & && \text{if } (t > t_{-0} + d) v = 0
 \end{aligned} \tag{14}$$

where  $u$  is the adaptive current (entirely defined by equation (14)),  $t_{-0}$  the last spiking time,  $d$  the non-linear current delay. The differential equation is simulated using an Euler interpolation as in (Izhikevich, 2003; Touboul, 2008) to compare our result to what has been obtained by the other authors. The obvious event-based simulation of this model has been also implemented<sup>5</sup>. The input current  $i$  is either a step or a ramp as detailed in Fig. 13 and Table 2.

Four parameters, the constant leak conductance  $g$ , the reversal potential  $E$ , the adaptation current  $k$  step and the (eventually infinite) non-linear current delay  $d$  allows to fix the firing regime. These parameters are to be recalculated after the occurrence of each internal or external spike. In the present context, it was sufficient to use constant value except for one regime, as made explicit in Fig. 2. We use the two-stages current whose action is to reset the membrane current after a certain delay. We made this choice because it was the simplest and leads to a very fast implementation.

Experimental results are given in Fig. 13 for the parameters listed in Fig. 2. These results correspond to almost all well-defined regimes proposed in (Izhikevich, 2003). The parameter adjustment is very easy, we in fact use parameters given in (Izhikevich, 2003) with some tiny adjustments. It is an interesting numerical result: The different regimes are generated by parameters values closed to those chosen for the quadratic model, the dynamic phase diagram being likely similar. See (Touboul, 2008) for a theoretic discussion.

This places a new point on the performance/efficiency plane proposed by (Izhikevich, 2004) at a very challenging place, and see that we can easily simulate different neuronal regimes with event-based simulations.

However, it is clear that such model does *not* simulates properly the neuron membrane potential as it is the case for the exponential model (Brette & Gerstner, 2005). It is usable if and only if spike emission is considered,

whereas the membrane potential value is ignored.

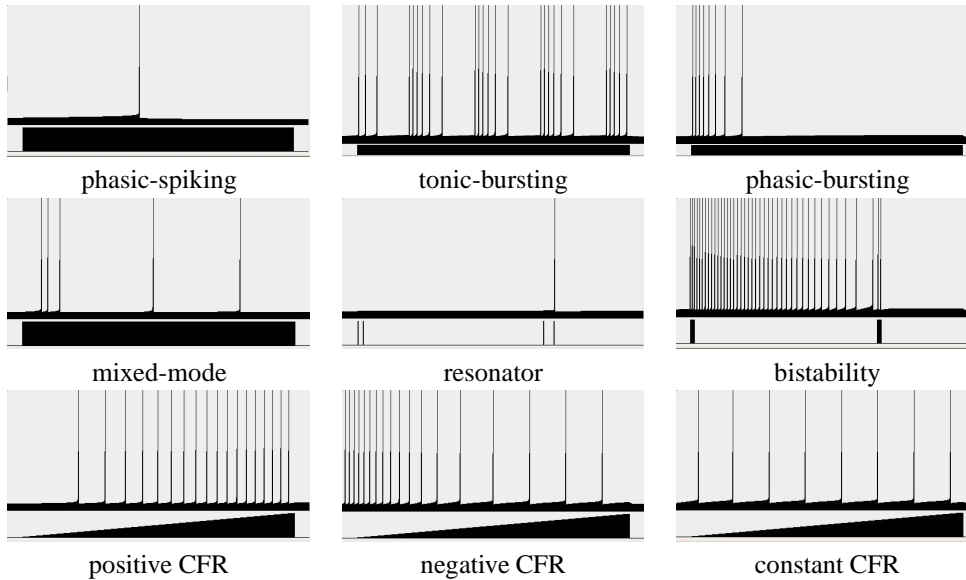


Figure 13: Typical results showing the versatility of the reduced model for spiking, bursting and other modes, including and different current-frequency-responses (CFR). For each mode, the upper trace shows the action potentials, the lower trace the input current. These results include the excitatory mode of type I where the spike frequency can be as small as possible in a  $1 - 10^3 Hz$  range and of type II where the spike frequency remains bounded. Tonic spiking is not shown, since obvious to obtain.

## References

- Amitai, Y., Gibson, J., Beirleiner, M., Patrick, S., Ho, A., B.W.Connors, et al. (2002). The spatial dimensions of electrically coupled networks of interneurons in neocortex. *J. Neurosci.*, 22, 4142–4152.
- Azouz, R., & Gray, C. (2000). Dynamic spike threshold reveals a mechanism for synaptic coincidence detection in cortical. In *Proceedings of the national academy of science* (Vol. 97, pp. 8110–8115).
- Baudot, P. (2007). *Nature is the code: high temporal precision and low noise in v1*. Unpublished doctoral dissertation.
- Brette, R. (2006). Exact simulation of integrate-and-fire models with synaptic conductances. *Neural Computation*, 18(8), 2004–2027.
- Brette, R. (2007). Exact simulation of integrate-and-fire models with exponential currents. *Neural Computation*, 19(10), 2604–2609.
- Brette, R., & Gerstner, W. (2005). Adaptive exponential integrate-and-fire model as an effective description of neuronal activity. *Journal of Neurophysiology*, 94, 3637–3642.
- Brette, R., Rudolph, M., Carnevale, T., Hines, M., Beeman, D., Bower, J. M., et al. (2007). Simulation of networks of spiking neurons: a review of tools and strategies. *Journal of Computational Neuroscience*, 23(3), 349–398.
- Burnod, Y. (1993). *An adaptive neural network: the cerebral cortex*. Masson, Paris. (2nd edition)

spiking mode	leak conductance $g$	reverse potential $E$	adaptation step $k$	non-linear delay $\tau$	input magnitude $i(\tau)$	input form
phasic-spiking	0.04	0	30	$+\infty$	0.5	step
tonic-bursting	0.18	1.6	14.6	60	15	step
phasic-bursting	0.06	11	11.2	$+\infty$	0.5	step
mixed-mode	0.01	0	$K$	150	10	step
resonator	0.04	-27	0	$+\infty$	38	bi-pulse
bistability	0.88	80	1.8	$+\infty$	65	pulse
positive CFR	0.01	0	0	$+\infty$	30	ramp
negative CFR	0.52	80	4	$+\infty$	30	ramp
constant CFR	0.52	0	4	100	30	ramp

Table 2: Examples of parameters used to generate the spiking modes shown in Fig. 13. The mixed mode is simulated by a variable adaptation step  $k = \{-20, 20\}$ .

- Carandini, M., Demb, J. B., Mante, V., Tollhurst, D. J., Dan, Y., Olshausen, B. A., et al. (2005, November). Do we know what the early visual system does? *Journal of Neuroscience*, 25(46), 10577–10597.
- Carandini, M., & Ferster, D. (2000). Membrane potential and firing rate in cat primary visual cortex. *The Journal of Neuroscience*, 20(1), 470–484.
- Cessac, B. (2008). A discrete time neural network model with spiking neurons. i. rigorous results on the spontaneous dynamics. *J. Math. Biology*, 56(3), 311–345.
- Cessac, B., & Samuelides, M. (2007). From neuron to neural networks dynamics. *EPJ Special topics: Topics in Dynamical Neural Networks*, 142(1), 7–88.
- Cessac, B., & Viéville, T. (2008, July). On dynamics of integrate-and-fire neural networks with adaptive conductances. *Frontiers in neuroscience*, 2(2).
- Connolly, C. G., Marian, I., & Reilly, R. G. (2004). Approaches to efficient simulation with spiking neural networks. In *Connectionist models of cognition and perception ii* (Vol. 15, pp. 231–240). World Scientific, London.
- Crook, S., Ermentrout, G., & Bower, J. (1998). Spike frequency adaptation affects the synchronization properties of networks of cortical oscillations. *Neural Computation*, 10(4).
- Dayan, P., & Abbott, L. F. (2001). *Theoretical neuroscience : Computational and mathematical modeling of neural systems*. MIT Press.
- Destexhe, A. (1997). Conductance-based integrate and fire models. *Neural Computation*, 9, 503–514.
- Destexhe, A., Rudolph, M., & Paré, D. (2003). The high-conductance state of neocortical neurons in vivo. *Nature Reviews Neuroscience*, 4, 739–751.
- Frégnac, Y. (2003). Association field in visual cortical neurons: From subthreshold visual synaptic integration to apparent-motion perception. In *European Conference on Visual Perception, Paris*.
- Frégnac, Y. (2004). From synaptic rumours to low-level perception: an intracellular view of visual cortical dynamics. *Progress in Biochemistry and Biophysics*, 31, 6–8.
- Galarreta, M., & Hestrin, S. (2001). Electrical synapses between gaba-releasing interneurons. *Nature Reviews Neuroscience*, 2, 425–433.
- Gautrais, J., & Thorpe, S. (1998). Rate coding vs temporal order coding : a theoretical approach. *Biosystems*, 48, 57–65.
- Gerstner, W., & Kistler, W. (2002). *Spiking neuron models*. Cambridge University Press.
- Hines, M., & Carnevale, N. (2004). Discrete event simulation in the neuron environment. *Neurocomputing*, 1117–1122.
- Hodgkin, A., & Huxley, A. (1952). A quantitative description of membrane current and its application to conduction and excitation in nerve. *Journal of Physiology*, 117, 500–544.

- Izhikevich, E. (2003). Simple model of spiking neurons. *IEEE Transactions on Neural Networks*, 14(6), 1569–1572.
- Izhikevich, E. (2004, September). Which model to use for cortical spiking neurons? *IEEE Trans Neural Netw*, 15(5), 1063–1070.
- Koch, C. (1999). *Biophysics of computation: Information processing in single neurons*. Oxford University Press: New York.
- Koch, C., & Segev, I. (Eds.). (1998). *Methods in neuronal modeling: From ions to networks*. The MIT Press.
- Lee, G., & Farhat, N. (2001). The double queue method: a numerical method for integrate-and-fire neuron networks. *Neural Networks*, 14(6-7), 921–932.
- Lewis, T. J., & Rinzel, J. (2003). Dynamics of spiking neurons connected by both inhibitory and electrical coupling. *Journal of Computational Neuroscience*, 14(3), 283-309.
- Maass, W. (1997). Fast sigmoidal networks via spiking neurons. *Neural Computation*, 9, 279–304.
- Maass, W., & Bishop, C. M. (Eds.). (2003). *Pulsed neural networks*. MIT Press.
- Maass, W., & Natschlagler, T. (1997). Networks of spiking neurons can emulate arbitrary hopfield nets in temporal coding. *Neural Systems*, 8(4), 355–372.
- Mainen, Z., & Sejnowski, T. (1995). Reliability of spike timing in neocortical neurons. *Science*, 268(5216), 1503-1506.
- Markram, H., Lübke, J., Frotscher, M., & Sakmann, B. (1997). Regulation of synaptic efficacy by coincidence of postsynaptic ap and epsp. *Science*, 275(213).
- Mattia, M., & Giudice, P. D. (2000). Efficient event-driven simulation of large networks of spiking neurons and dynamical synapses. *Neural Computation*, 12, 2305-2329.
- McCormick, D. A., & Bal, T. (1997). Sleep and arousal: Thalamocortical mechanisms. *Annual Review of Neuroscience*, 20, 185-215.
- Morrison, A., Mehring, C., Geisel, T., Aertsen, A., & Diesmann, M. (2005). Advancing the boundaries of high connectivity network with distributed computing. *Neural Comput*, 17(8), 1776–1801.
- Morrison, A., Straube, S., Plesser, H., & Diesmann, M. (2007). Exact subthreshold integration with continuous spike times in discrete-time neural network simulations. *Neural Computation*, 19, 47–79.
- Mouraud, A., Puzenat, D., & Paugam-Moisy, H. (2005). *Damned: A distributed and multithreaded neural event-driven simulation framework* (Tech. Rep. No. hal-00015137). HAL CNRS.
- Par, D., Bouhassira, D., Oakson, G., & Datta, S. (1990). Spontaneous and evoked activities of anterior thalamic neurons during waking and sleep states. *Experimental Brain Research*, 80(1).
- Pfister, J.-P., & Gerstner, W. (2006). Triplets of spikes in a model of spike timing-dependent plasticity. *J. Neurosci.*, 26, 9673–9682.
- Rieke, F., Warland, D., Steveninck, R. de Ruyter van, & Bialek, W. (1996). *Spikes, exploring the neural code*. The M.I.T. Press.
- Rochel, O., & Martinez, D. (2003). An event-driven framework for the simulation of networks of spiking neurons. In *Proc. 11th european symposium on artificial neural networks* (pp. 295–300).
- Rotter, S., & Diesmann, M. (1999). Exact digital simulation of time-invariant linear systems with application to neuronal modeling. *Biol. Cybern.*, 81, 381–402.
- Rudolph, M., & Destexhe, A. (2006). Analytical integrate and fire neuron models with conductance-based dynamics for event driven simulation strategies. *Neural Computation*, 18, 2146–2210.
- Rudolph, M., & Destexhe, A. (2007). How much can we trust neural simulation strategies? *Neurocomputing*. (To appear)
- Ruf, B. (1998). *Computing and learning with spiking neurons - theory and simulations*. Unpublished doctoral dissertation, Institute for Theoretical Computer Science, Univ. Graz, Austria.

- Schrauwen, B. (2007). *Towards applicable spiking neural networks*. Unpublished doctoral dissertation, Universiteit Gent, Belgium.
- Simoncelli, E., & Olshausen, B. (2001). Natural image statistics and neural representation. *Annual Review of Neuroscience*, 24(1), 1193–1216.
- Thorpe, S., & Fabre-Thorpe, M. (2001). Seeking categories in the brain. *Science*, 291, 260–263.
- Touboul, J. (2008). Bifurcation analysis of a general class of non-linear integrate and fire neurons. *SIAM Journal of Applied Mathematics*, 68(4), 1045–1079.
- Viéville, T., Chemla, S., & Kornprobst, P. (2007). How do high-level specifications of the brain relate to variational approaches? *Journal of Physiology - Paris*, 101(1-3), 118–135.
- Viéville, T., & Crahay, S. (2004). Using an hebbian learning rule for multi-class svm classifiers. *Journal of Computational Neuroscience*, 17(3), 271–287.
- Viéville, T., & Rochel, O. (2006). One step towards an abstract view of computation in spiking neural-networks. In *International conf. on cognitive and neural systems*.
- Wohrer, A., & Kornprobst, P. (2008). Virtual Retina : A biological retina model and simulator, with contrast gain control. *Journal of Computational Neuroscience*. (DOI 10.1007/s10827-008-0108-4)

**Acknowledgment:** Partially supported by the ANR MAPS & the MACCAC ARC projects.

**current**

21

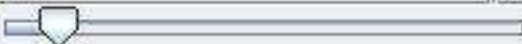


**current form**

- step
- ramp
- pulse
- bi-pulse

**conductance**

0.2



**reversal potential**

-65.6



**adaptation**

0



**non-linear latency**

2000



**chosen model**

- yvette
- izhikevich

**modes**

tonic-spiking



Show the temporal response

